Penetration depth for shallow impact cratering

M. A. Ambroso,[1] C. R. Santore,[1] A. R. Abate,[1,2] and D. J. Durian[1,2]
[1]*Department of Physics and Astronomy, University of California, Los Angeles, California 90095-1547, USA*
[2]*Department of Physics and Astronomy, University of Pennsylvania, Philadelphia, Pennsylvania 19104-6396, USA*
(Received 10 November 2004; revised manuscript received 7 February 2005; published 17 May 2005)

We present data for the penetration of a variety of spheres, dropped from rest, into a loose noncohesive granular medium. We improve upon earlier work [J. S. Uehara *et al.*, Phys. Rev. Lett. **90**, 194301 (2003)] in three regards. First, we explore the behavior vs sphere diameter and density more systematically, by holding one of these parameters constant while varying the other. Second, we prepare the granular medium more reproducibly and, third, we measure the penetration depth more accurately. The new data support the previous conclusion that the penetration depth is proportional to the $1/2$ power of sphere density, the $2/3$ power of sphere diameter, and the $1/3$ power of total drop distance.

DOI: 10.1103/PhysRevE.71.051305 PACS number(s): 45.70.Ht, 45.70.Cc, 83.80.Fg, 89.75.Da

The mechanics of granular media continue to defy our intuition. In spite of their ubiquity in everyday life and industry, we have no fully reliable rules for predicting response to an applied force [1–3]. If the forcing is weak, the medium remains at rest and the local disorder in the packing gives rise to ramified force chains with structures much larger than the grain size. If the forcing is strong, the medium can flow. But when will the medium yield? Will the flow be smooth or intermittent? How do velocity and density vary with position and time? No experimental characterization currently exists that can be used to predict response in all other sample and forcing geometries. For example, flow down an incline offers little insight as to how the same medium would flow between rotating cylinders or on a vibrated plate.

Recently we investigated the mechanics of impact by projectiles dropped into granular media [4,5]. This is a situation of natural interest. Some of us would like to understand how far our feet sink into the sand when walking, running, or jumping at the beach. Others of us would like to understand the lie of our golf ball in a sand trap. Still others would like to know how far a warhead can penetrate the earth prior to detonation [6]. It is also interesting to consider the effect of impact on the medium itself: the nature of the granular splash [7,8] and the morphology of the resulting crater [9–15]. Our motivation is more general: to find a noncontrived situation permitting the unusual nature of granular mechanics to be both highlighted and characterized. Projectile impact is ideal on both counts. It is interesting that penetration is nonzero even for near-zero impact speed, but grows only very slowly with projectile energy. The average stopping force $\langle F\rangle$ can be very small, but can also increase dramatically for stronger impacts. This unusual mechanics can be studied quantitatively from the penetration depth d via a simple statement of energy conservation:

$$\langle F\rangle = mgH/d, \tag{1}$$

where m is the projectile mass, $g=9.8\ \mathrm{m/s^2}$, and H is the total drop distance. Note that H is the sum of the free-fall height h and the penetration depth d (see inset of Fig. 1).

In Ref. [4] we measured the penetration of spherical projectiles of various densities ρ_b, and diameters D_b, into loose noncohesive granular media of various densities ρ_g and angles of repose $\tan^{-1}\mu$. In all cases the minimum free fall height was nearly zero, and the maximum penetration depth was comparable to the ball diameter. All of our data collapsed according to an empirical scaling relation,

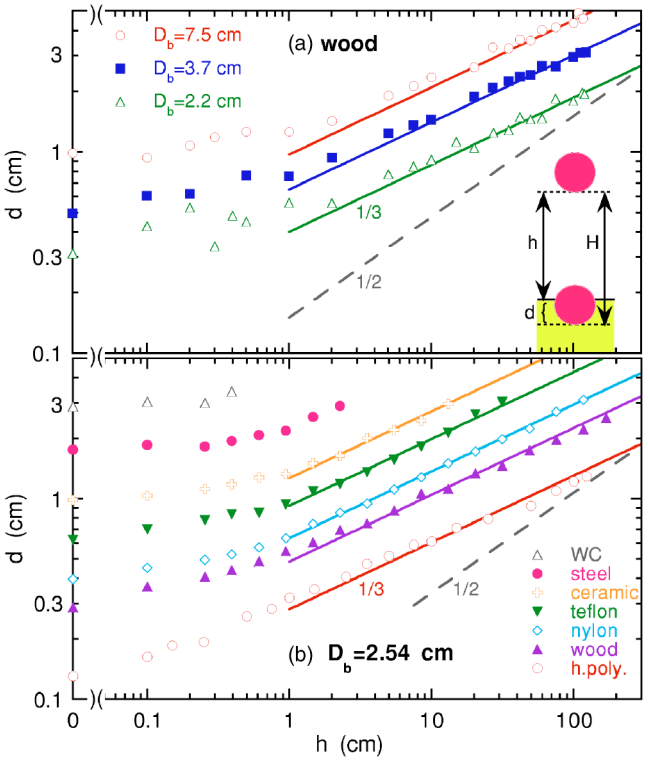

FIG. 1. Penetration depth d vs free-fall height h for (a) wooden spheres of different diameter and (b) one-inch spheres of different density. The granular medium is postfluidized glass beads of diameter range 0.25–0.35 mm. The projectile materials and densities are as follows: hollow polypropylene, 0.28 $\mathrm{g/cm^3}$; wood, 0.7 $\mathrm{g/cm^3}$; nylon, 1.2 $\mathrm{g/cm^3}$; teflon, 2.2 $\mathrm{g/cm^3}$; ceramic, 3.8 $\mathrm{g/cm^3}$; steel, 7.8 $\mathrm{g/cm^3}$; tungsten carbide (WC), 15 $\mathrm{g/cm^3}$.

$$d = 0.14\frac{1}{\mu}\left(\frac{\rho_b}{\rho_g}\right)^{1/2} D_b^{2/3} H^{1/3}. \quad (2)$$

In Ref. [5] we showed how this naturally generalizes to cylindrical projectiles, independent of the tip shape. If true, Eq. (2) has several interesting implications. First, it implies via Eq. (1) that the average stopping force is proportional to the tangent of the repose angle, μ, consistent with the notion that it represents a friction coefficient [1]. Second, it implies that the granular medium can be extremely fragile, suffering a nonzero penetration even for zero free-fall height. Equation (2) gives this minimum penetration as

$$d_\circ = (0.14/\mu)^{3/2}(\rho_b/\rho_g)^{3/4} D_b. \quad (3)$$

The penetration depth formula then can be recast dimensionlessly as $d/d_\circ = (H/d_\circ)^{1/3}$. Third, since Eq. (2) is dimensionally complete, it suggests that the effects of grain-grain cohesion and interstitial air are both negligible. If they were not, then even further physics would have to enter to cancel the extra units. Air and cohesion effects can also be ruled out because we found identical penetrations for granular media that are identical except for particle sizes [4]. This is to be expected, according to the Geldart classification scheme of fluidization behavior vs particle size and density [16]. Fourth, and perhaps most curious, Eq. (2) implies that the penetration is not a function of either impact energy, $\sim \rho_b h$, or impact momentum, $\sim \rho_b h^{1/2}$.

The penetration of projectiles into granular media has also been measured recently by other groups [17–19]. Ciamarra *et al.* [17] performed quasi-two-dimensional experiments in which a steel cylinder was dropped sideways into a packing of rods. The impact speeds varied by about a factor of five, and the penetration depths varied from about 1.5 to 7 times the projectile diameter. They report that the projectile deceleration is time-independent and proportional to the impact speed. This implies that the stopping time is constant and that the penetration depth is proportional to the impact speed. de Bruyn and Walsh [18] performed experiments in which two different diameter steel spheres were dropped into glass spheres of five different bead sizes. The impact speeds varied by about a factor of four, and the penetration depths varied from about 1.2 to 5 times the projectile diameter. They report that the penetration depth is linear in impact speed, but with an intercept $d_\circ$ that can be positive or negative. This is modelled in terms of a Bingham fluid, where the granular medium exerts a force on the projectile according to a yield stress and an effective viscosity, $F(v) = -F_\circ - bv$. Negative intercepts for depth vs speed are predicted by this model. Even more recently Lohse *et al.* [19] performed experiments in which spheres are dropped at zero free-fall height ($h=0$), just barely touching the sand. The projectile densities varied widely, at fixed diameter, giving penetration depths $d_\circ$ ranging from about $1/4$ to 6 times the ball diameter. They report that the minimum penetration is linear in projectile density. This is modelled in terms of Coulomb friction, where the medium exerts a force on the projectile proportional to its depth, $F(z) = -kz$. Including gravity, this law predicts the penetration depth for nonzero drop heights to be $d/d_\circ = (H/d_\circ)^{1/2}$.

To summarize published results for the dependence on drop height, $d \sim H^{1/3}$ was reported in our first paper [4], whereas $d \sim v_\circ \sim h^{1/2}$ was found in Ref. [17] and $d - d_\circ \sim h^{1/2}$ was found in Ref. [18]. By comparison with the projectile diameter, the penetrations are shallow in Ref. [4] but deep in Refs. [17,18]. Thus there may be no conflict; the experiments could simply fall into different scaling regimes. However, evidence of $d \sim H^{1/3}$ for deeper penetrations of cylinders is reported in [5]. Furthermore, Ref. [18] states that our shallow penetration depth data of [4] are well described by their model. This raises the possibility that our respective data sets are actually consistent, and that one of us is mistaken as to the specific power-law behavior.

The published results for the dependence on projectile density are also not in agreement. Our scaling law implies $d_\circ \sim {\rho_b}^{3/4}$ for $h=0$, Eq. (3), whereas $d_\circ \sim \rho_b$ is reported in Ref. [19]. Again the penetrations are more shallow in our work, so the respective experiments may simply be in different scaling regimes. Furthermore, our beads are large enough that grain-grain cohesion is negligible, whereas the grain size and packing fraction are both considerably smaller in Ref. [19]. To date, we are the only group to report density scaling for $h > 0$.

Altogether, the results of Refs. [4,17–19] suggest that there may be three distinct sets of impact behavior. (1) Shallow penetration into noncohesive media, where Eq. (2) holds [4]; (2) Deep penetration into noncohesive media, where $d - d_\circ \sim v_\circ$ and $F(v) = -F_\circ - bv$ hold [17,18]; and (3) penetration into small tenuously packed grains, where $F(z) = -kz$ holds [19].

In this paper we (1) provide more details for our original Letter [4], and we (2) report on experiments designed to clarify the experimental situation for shallow impacts. Our approach is both to improve the reproducibility and accuracy of the measuring apparatus, and to systematically and widely vary the drop distance, the ball diameter, and the ball density. We also adopt the gas-fluidization preparation method, to see if it changes the scaling. We shall demonstrate that the deviations of data from Eq. (2) are mainly statistical. We shall also demonstrate that better collapse can be achieved by Eq. (2) than by the impact speed scaling of Refs. [17,18]. This reaffirms the correctness of our original work, Refs. [4,5], and negates the statement in Ref. [18] that our results can be described by their model.

I. METHODS

Our granular medium is P-0140 A-Series technical quality solid glass spheres from Potters Industries Inc. (PA). The beads are slightly polydisperse, with a diameter range of 0.25–0.35 mm as set by US sieve sizes 45–60. The quoted density of the glass material is 2.5 g/cc. In our previous work [4,5], we poured the beads into a beaker and then gently swirled and tapped it to achieve a horizontal surface and a random close packing fraction of about 0.64. In case this led to irreproducibility of packing or surface angle, we now prepare the system by air-fluidization. The sample container consists of a plexiglass tube with 8-inch outer diameter, $1/4$-inch wall thickness, and 5-ft height. The top is open to

air, while the bottom consists of a Brass sieve with 90 μm mesh opening. Under the sieve is a windbox consisting of a plexiglass tube of same diameter but 12-inch height. The glass beads are poured onto the sieve to a depth of approximately 8 inches. Dry air is then blown at high rate into the bottom of the windbox, and up through the glass beads, until all fines and humidity are removed. Prior to each drop, the beads are more gently fluidized, and the airflow is gradually reduced, so that a flat level surface remains. It is crucial to turn down the airflow very slowly, in order to avoid large gas bubbles that leave behind surface irregularities. In earlier work [20] we found that this procedure gives a packing fraction of 0.590 ± 0.004, as expected for hard noncohesive spheres.

We employ two series of spherical projectiles. The first is wooden spheres of density $\rho_b = 0.7$ g/cc and varying diameter: $D_b = \{1/4, 1/2, 5/8, 7/8, 1, 3/2, 2, 3\}$ inches. The second is 1-inch diameter spheres of varying density: hollow polypropylene, 0.28 g/cc; wood, 0.7 g/cc; nylon, 1.2 g/cc; teflon, 2.2 g/cc; ceramic, 3.8 g/cc; steel, 7.9 g/cc; tungsten carbide (WC), 15 g/cc. These are held and dropped with zero speed from the center of the sample tube using a suction mechanism. In comparison with our previous work [4], the new sample dimensions and maximum ball diameter are all about twice as great, but the maximum drop heights are comparable. Since the penetration depth grows less than linearly with ball diameter, we judge that sample-size effects are negligible. Furthermore, we never observe any grain movement at the edge of the sample as a result of impact.

The height of the sand surface, the height of the bottom of the ball prior to drop, and the height of the top of the ball after the drop, are all measured using a microtelescope (Titan Tool Supply, Cathetometer TC-11) mounted to a height gauge. The sample container and height gauge are approximately 1-foot apart, both resting on an optical bench. From the height gauge readings, we deduce the free-fall height h, the penetration depth d, and the total drop distance $H = h + d$. This method permits study of penetrations no deeper than the ball diameter, since the top of the ball must be visible from the side. For slightly deeper penetrations, until the ball becomes fully buried, we estimate the depth from the height of the suction mechanism when it is brought into contact with the top of ball.

II. RESULTS

Raw data for penetration depth vs free-fall height are displayed on a log-log plot in Fig. 1 for three example wooden spheres and for all 1-inch spheres. The minimum penetration depth, $d_\circ$ for $h = 0$, where the ball bottom was initially just in contact with the sand surface, is displayed along the left axis. For decreasing h, the penetration depths extrapolate smoothly to the $h = 0$ limit. For increasing h, the data appear to approach a $1/3$ power law, shown in Fig. 1 by solid lines. There is no evidence of $h^{1/2}$ behavior, given by the dashed lines, which would correspond to the $d \sim v_\circ$ scaling of Ref. [17]. Figure 1 demonstrates clearly that d cannot be a power-law over the full range of h due to the nonzero intercept, $d_\circ > 0$. One possibility for simple scaling is that d is a power of total drop distance, $H = h + d$, as advocated in Ref. [4]. Another is that $d - d_\circ$ is a power of the free-fall distance h, as advocated in Ref. [18]. In the next sections we investigate both these possibilities.

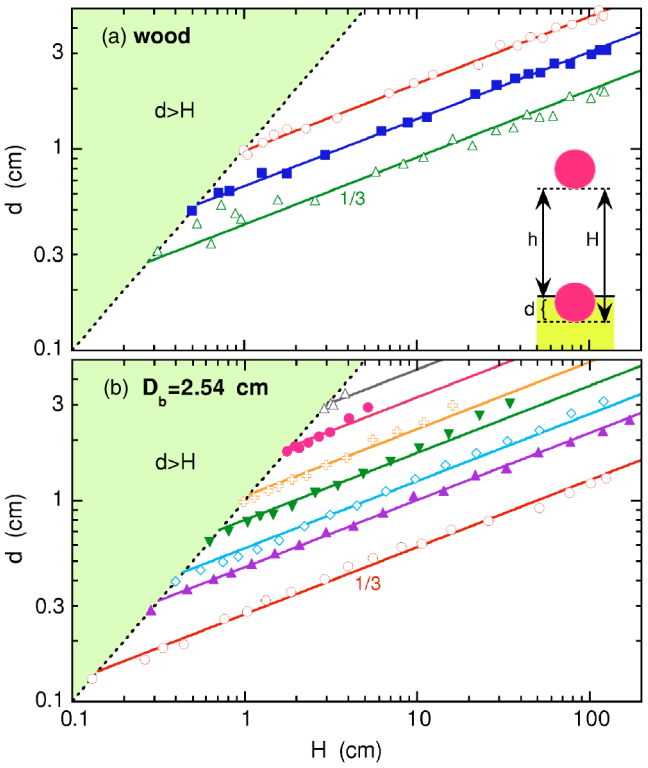

FIG. 2. Penetration depth d vs total drop distance H for (a) wooden spheres of different diameter, and (b) one-inch spheres of different density. The symbol code is the same as in Fig. 1. The solid lines are the best fits to $d \propto H^{1/3}$. Note that the shaded region, $d > H$, is forbidden.

III. TOTAL DROP DISTANCE SCALING

The total drop distance, $H = h + d$, is a relevant parameter because it relates to the average stopping force via Eq. (1). Thus, in Fig. 2, we replot all the penetration data of Fig. 1 vs H. Now the minimum penetration data points, for free-fall height $h = 0$, lie along the line $d = H$; no data may lie in the shaded region $d > H$. Whereas in Fig. 1 the data trended toward $d \sim h^{1/3}$ for large drop heights, now in Fig. 2 all the data lie along $d \sim H^{1/3}$ power laws. For the lighter spheres, which never submerge, the deviation from power-law behavior is purely statistical. For these data sets, the dynamic range in H is two to three decades, enough to give confidence in form and a few percent uncertainty in exponent. For denser spheres, the $H^{1/3}$ power-law fits gives an acceptable description, but may deviate for penetrations deeper than about a ball diameter.

The power-law behavior of Fig. 2 is further analyzed in Fig. 3, where we plot the proportionality constant of the power-law fits, $d/H^{1/3}$, as a function of projectile properties. In the top plot, Fig. 3(a), we display results for the wooden spheres vs their diameter. Note that three of the points cor-

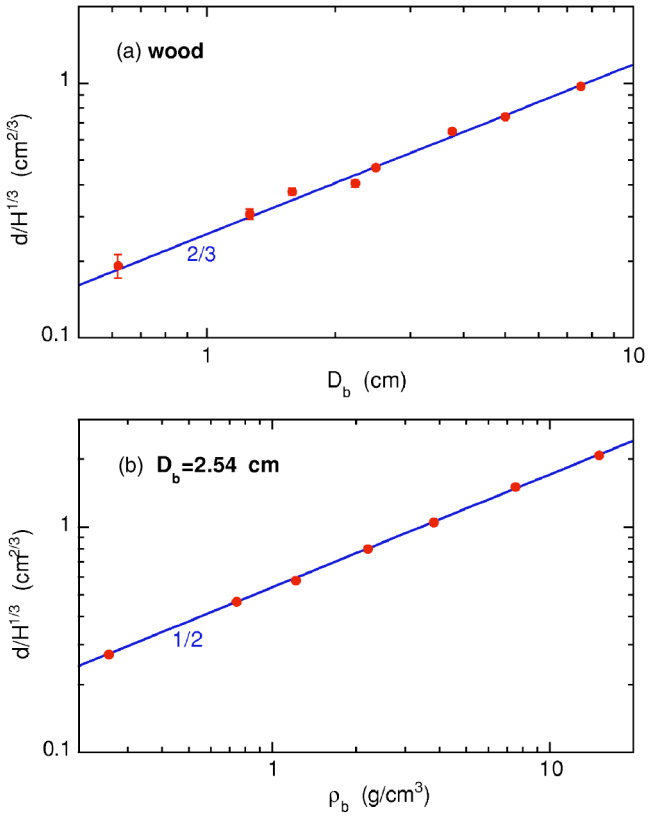

FIG. 3. Scaled penetration depth vs (a) projectile diameter and (b) projectile density. Each point corresponds to a fit to $d \propto H^{1/3}$ as shown in Fig. 2. The solid lines are the best power-law fits, giving exponents of (a) 2/3 for diameter and (b) 1/2 for density.

respond to the three example data sets and fits shown in Fig. 2(a). Evidently, to within statistical uncertainty, the penetration depth scales as the 2/3 power of projectile diameter with a dynamic range of slightly over one decade. The penetration depth thus scales as $d \sim D_b^{2/3} H^{1/3}$. This expression is dimensionally correct, which suggests that we have empirically uncovered most of the physics. In other words, the observed $D_b^{2/3}$ scaling lends support to our claim of $H^{1/3}$ scaling.

In Fig. 3(b) we display the proportionality constant of the power law fit, $d/H^{1/3}$, for all the one-inch spheres as a function of their density. Each point corresponds to one data set and fit in Fig. 2(b). Evidently, to within statistical uncertainty, the penetration depth scales as the square-root of projectile density with a dynamic range of over one and one half decades. We find the same density dependence as the jet penetration formula [10].

Before closing this section, we offer an alternative means of analyzing penetration data in terms of total drop distance. As noted in the introduction, Eq. (2) can be recast as $d/d_\circ = (H/d_\circ)^{1/3}$, where $H = h + d$, h is the free-fall height, and $d_\circ$ is the minimum penetration depth for $h = 0$. Thus in Fig. 4 we check for data collapse by plotting $d/d_\circ$ vs $H/d_\circ$, using measured values of $d_\circ$. The scatter of data is not negligible, but the average is well described by the expected 1/3 power law, shown as a solid blue curve. Even tighter collapse onto this curve can be achieved if $d_\circ$ is treated as an adjustable parameter. For comparison, the $d/d_\circ = (H/d_\circ)^{1/2}$ power law predicted by the model of Ref. [19] is shown as a dashed green curve. For both this model and our observations, $d_\circ$ is the crucial length scale characteristic of a particular system of projectile and granular medium. The value of $d_\circ$ is proportional to the projectile diameter, D_b, and a power of the projectile:medium density ratio, ρ_b/ρ_g. The inset of Fig. 4 shows our data for $d_\circ$ vs ρ_b, for all $D_b = 2.54$ cm spheres. The results are consistent with our expectation, $d_\circ \sim \rho_b^{3/4}$ Eq. (3). For comparison, the $d_\circ \sim \rho_b$ observation of Ref. [19] is shown as a solid green curve. We speculate that the small particle size and the very tenuous packing in Ref. [19] are responsible for the different behavior.

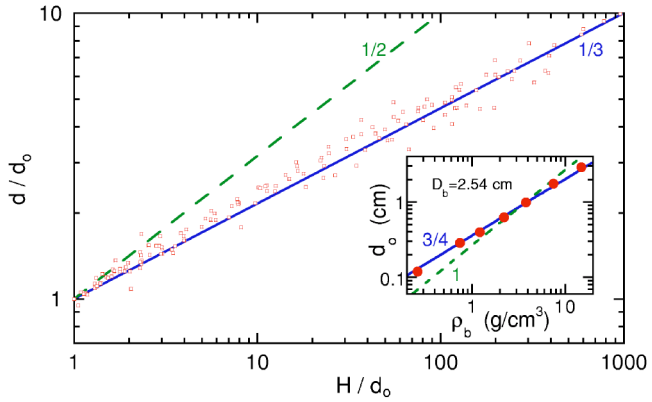

FIG. 4. All the penetration depth data of Fig. 1, vs total drop distance, both scaled by minimum penetration depth. The data all collapse onto $d/d_\circ = (H/d_\circ)^{1/3}$ (solid blue curve), expected from Eqs. (1) and (2). The characteristic length scale, $d_\circ$, scales with projectile diameter and the 3/4 power of projectile density (inset, solid blue curve). By comparison, $d/d_\circ = (H/d_\circ)^{1/2}$ and $d_\circ \sim \rho_b$ are predicted by the model of Ref. [19] (dashed green curves).

Altogether Figs. 2–4 show quite convincingly that the penetration depth scales as

$$d \sim \rho_b^{1/2} D_b^{2/3} H^{1/3}, \tag{4}$$

in accord with Eq. (2). The demonstration here is stronger than in our prior work, Ref. [4], because the dynamic ranges are larger and the statistical uncertainties are smaller. But more importantly, the demonstration is stronger than in Ref. [4] because here the projectile diameters and densities are varied more systematically, with one held fixed while the other is changed. Nonetheless, Ref. [4] still complements the present work in that it established the dependence of penetration on the properties of the granular medium via Eq. (2) as $d \sim 1/(\mu \rho_g^{1/2})$.

IV. IMPACT SPEED SCALING

In Refs. [17,18], penetration depth data are reported to scale according to impact speed rather than by Eq. (2). Furthermore, Ref. [18] reports that our earlier data also can be scaled by impact speed. Therefore in this section we attempt to analyze our new data similarly. We begin with Fig. 5, where the penetration depth data of Fig. 1 are replotted as a function of impact speed, $v_\circ = \sqrt{2gh}$. Contrary to the sugges-

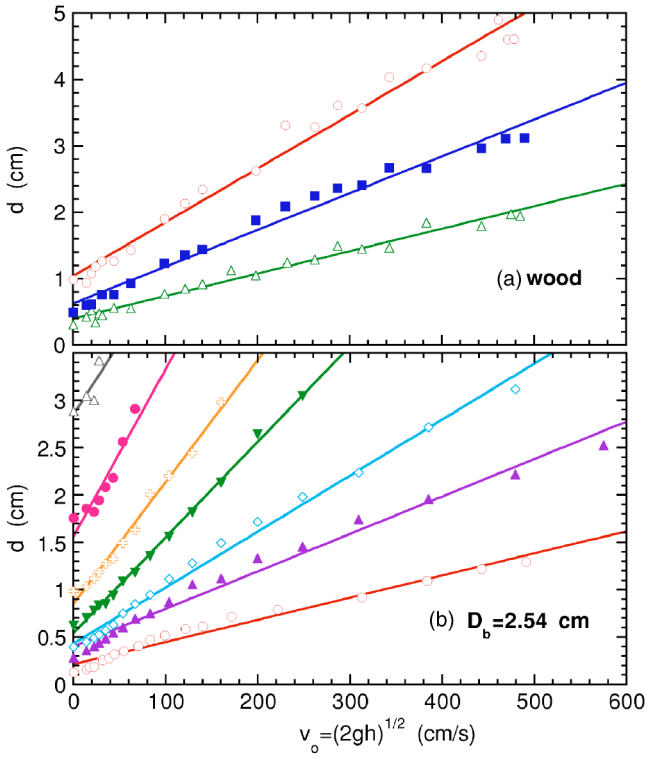

FIG. 5. Penetration depth vs impact speed for (a) wooden spheres of different diameter and (b) one-inch spheres of different density. The symbol code is the same as in Fig. 1. The solid lines are the best fits to $d=d_{\circ v}+v_{\circ}\tau$, where both $d_{\circ v}$ and τ are fitting parameters.

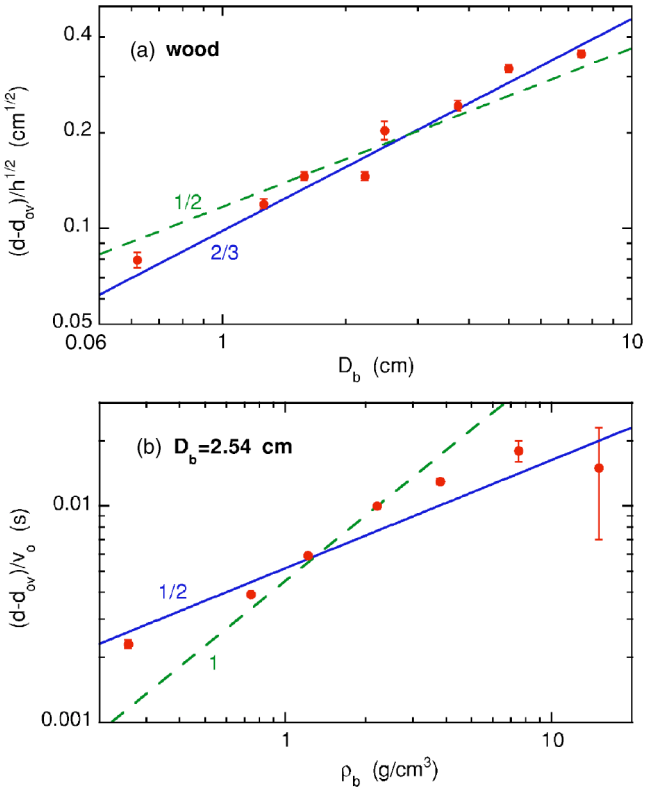

FIG. 6. Scaled penetration depth vs (a) projectile diameter and (b) projectile density. Each point corresponds to a fit to $d=d_{\circ v}+v_{\circ}\tau$ as shown in Fig. 5. The solid lines are the best power-law fits, giving exponents of (a) 2/3 for diameter and (b) 1/2 for density. The dashed lines represent dimensionally simpler expectations, but are not consistent with the data.

tions of Refs. [17,18], our data do not lie along the best line fits to $d=d_{\circ v}+v_{\circ}\tau$. For lighter spheres the data all curve downwards, while for denser spheres the data all curve upwards. Over a subset of speeds, e.g., $50\ \mathrm{cm/s}<v_{\circ}<400\ \mathrm{cm/s}$ as in Ref. [17], the fit to a straight line is satisfactory to within experimental uncertainty.

To see if we can make sense of the displayed fits to $d=d_{\circ v}+v_{\circ}\tau$, we examine *one* of the fitting parameters in Fig. 6 as a function of projectile properties. The top plot in shows $(d-d_{\circ v})/h^{1/2}$, i.e., the fitting parameter τ times $\sqrt{2g}$, as a function of ball diameter. A reasonable power-law fit can be made to ${D_b}^{2/3}$, which curiously is the same diameter exponent as Eq. (2). Though this fit gives a fine description, it is not dimensionally simple. If $(d-d_{\circ v})\propto {D_b}^{2/3}h^{1/2}$ is true, then there must be another important length scale in the problem that enters the proportionality constant. It would have been simpler had we found $(d-d_{\circ v})/h^{1/2}\propto {D_b}^{1/2}$, shown by a dashed line. Such behavior clearly differs from the data.

The bottom plot of Fig. 6 shows the fitting parameter $\tau=(d-d_{\circ v})/v_{\circ}$ as a function of ball density. The results curve downwards, and cannot be very well described by a power law. Nonetheless, the best power-law fit would be to ${\rho_b}^{1/2}$, as shown by the solid line. Curiously, the density exponent is the same as in Eq. (2). If true, this corresponds to scaling with the square root of impact energy, $(d-d_{\circ v})\sim\sqrt{\rho_b {v_{\circ}}^2}$. Scaling with impact momentum, suggested in the abstract of Ref. [18], would correspond to $(d-d_{\circ v})\sim\rho_b v_{\circ}$ as shown by the dashed line. Such behavior is vastly different from the data. Contrary to the abstract, however, the final scaling advocated in Ref. [18] is $(d-d_{\circ v})\sim{\rho_b}^{1/2}v_{\circ}$. This corresponds to the solid curve in Fig. 6(b), which still is not a satisfactory fit. Even better powerlaw fits can be made in both Figs. 6(a) and 6(b) if the last point is omitted; however, the resulting exponents do not lead to dimensionally simple scaling. While Figs. 5 and 6 alone do not unequivocally rule out scaling by impact speed, the contrast with scaling by total drop distance in Figs. 2 and 3 is striking.

Altogether, the best description of our new data in terms of impact speed is

$$d-d_{\circ v}\propto {\rho_b}^{1/2}{D_b}^{2/3}h^{1/2}, \tag{5}$$

where the intercept, $d_{\circ v}>0$, is a free fitting parameter as yet unaccounted for. According to the model of Ref. [18], the intercept can be explained by a yield stress but only if it is negative, which is not the case for our experiments. If Eq. (5) is true, the combined density and free-fall height dependencies imply that impact energy is the crucial parameter, not the impact momentum. For a complete understanding, one would still have to account for both the free parameter $d_{\circ v}$ as well as an additional length scale in the proportionality constant.

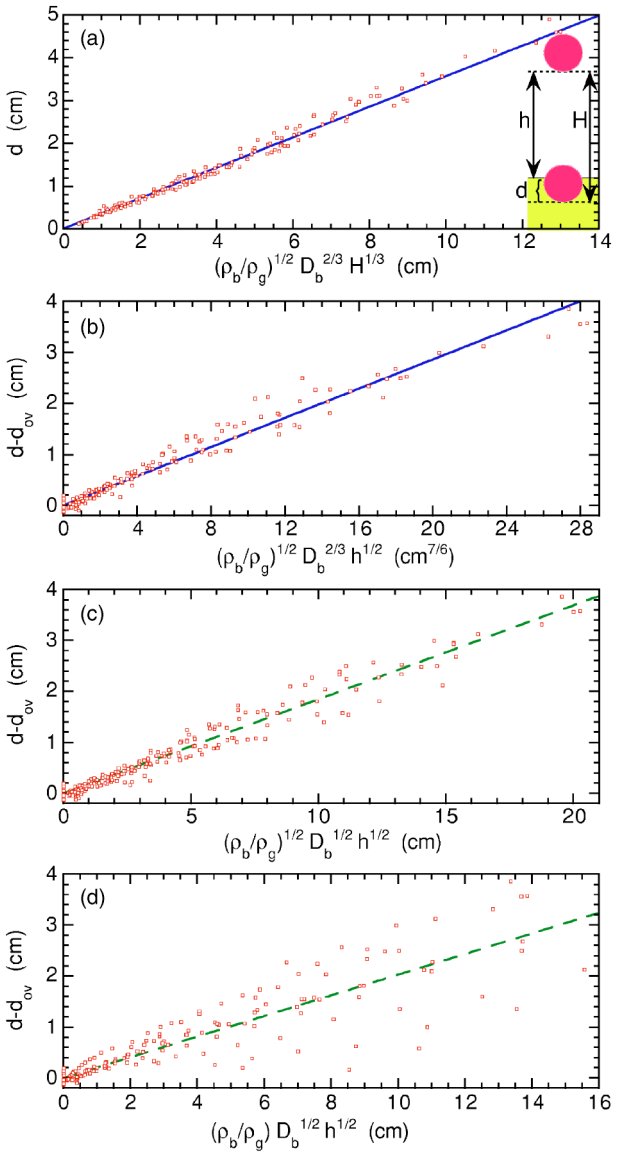

FIG. 7. Penetration depth vs (a) scaled total drop distance and (b)–(d) scaled free-fall height. In (a), the exponents for sphere density, sphere diameter, and total drop distance are taken from the fits of Figs. 2 and 3. In (b), the exponents are taken from the fits of Figs. 5 and 6. In (c), the exponents are taken according to the final prescription of Ref. [18]. In (d), the exponents are taken such that the x axis is a length scale proportional to impact momentum. In (b)–(d), $d_{\circ v}$ is a fitting parameter from Fig. 5 that is systematically different from the penetration depth at zero impact speed.

V. DATA COLLAPSE

As an alternative means to compare the relative quality of candidate scaling descriptions, we now attempt to collapse the penetration depth data of Fig. 1 according to both the total drop distance H as well as according to the impact speed $v_\circ = \sqrt{2gh}$. For collapse via Eq. (4), we plot penetration depths vs $(\rho_b/\rho_g)^{1/2} D_b^{2/3} H^{1/3}$ in Fig. 7(a). Though the grain density has not been explicitly varied here, we assume the same dependence as observed in Ref. [4]; this renders the x axis dimensionally correct. Evidently, in Fig. 7(a), the data collapse tightly to a straight line with a statistical deviation that is roughly a constant percentage. Assuming a proportionality constant of $0.14/\mu$, as in Eq. (2), we find that the repose angle of the postfluidized glass beads is $\theta_r = 21°$. This is slightly smaller than the value measured in Ref. [4] for glass beads at random close packing, $\theta_r = 24°$, as expected.

For collapse via Eq. (5), we subtract the *fitted* intercept from the penetration depths and plot vs $(\rho_b/\rho_g)^{1/2} D_b^{2/3} h^{1/2}$ in Fig. 7(b). The degree of collapse is noticeably not as tight as in Fig. 7(a), with a percentage deviation that blooms for smaller penetrations. Relatedly, the systematic curvature of the data away from $(d - d_{\circ v}) \propto h^{1/2}$, seen in Fig. 5(b), is reflected here by a deviation of the actual penetration depth for $h = 0$ from the value of the fitting parameter $d_{\circ v}$. If instead we plot $d - d_\circ$, where $d_\circ$ is the actual observed penetration for $h = 0$, then the degree of collapse in Fig. 7(b) is notably worse. Also, consistent with the diameter and density dependence shown in Fig. 6, the degree of collapse is worse in Fig. 7(c) when the penetration depth is plotted vs $(\rho_b/\rho_g)^{1/2} D_b^{1/2} h^{1/2}$, the final scaling advocated in Ref. [18].

Finally, in Fig. 7(d), we make one last attempt at collapsing our data. The abstract of Ref. [18] states that "…the penetration depth of the spheres increases linearly with the incident momentum of the projectile, but with a zero-momentum intercept that can be positive or negative." According to this prescription, we subtract the fitted intercept and plot the otherwise-raw penetration depth data of Fig. 1 vs the dimensionally-simplest quantity proportional to momentum: $(\rho_b/\rho_g) D_b^{1/2} h^{1/2}$. This gives a nearly random scattering of data points without the least hint of collapse. Thus, impact momentum does not determine the penetration depth for our data.

VI. CONCLUSION

Our new data for the shallow penetration of spheres into a loose granular medium strongly support our previous conclusions, Eq. (2), for the scaling of penetration depth. By improving preparation reproducibility and measurement accuracy, we demonstrate that the depth scales as the $1/3$ power of the total drop distance H. In particular there is a nonzero penetration even for zero drop height h, where the penetration depth equals the total drop distance. By systematically varying the projectile diameter at fixed density, and by systematically varying the projectile density at fixed diameter, we demonstrate that the depth scales as the $1/2$ power of projectile density and the $2/3$ power of projectile diameter. And by changing the sample preparation from random close packing in Ref. [4] to a random loose packing here, we demonstrate that sample preparation plays no crucial role. As long as the medium is loose and noncohesive, Eq. (2) should apply though with a value of μ that reflects the packing state. The burning question is now the nature of the granular mechanics that gives rise to this reaffirmed scaling behavior. The force law cannot be as suggested in Ref. [18], where the impact momentum of the projectile and a yield stress for the granular medium are crucial inputs. The positive intercept for penetration depth vs drop height, and the scaling with total drop distance H rather than with free-fall height h, sug-

gest instead that the stopping force may depend on the projectile's instantaneous depth as well as its speed. Such a scenario would be more in line with recent reports of the hydrostaticlike nature of the force on an object moving horizontally [21] or vertically [19,22] through a granular medium.

ACKNOWLEDGMENTS

This material is based upon work supported by the National Science Foundation under Grant No. DMR-0305106. We thank J.R. de Bruyn and D. Lohse for helpful conversations.

[1] R. L. Brown and J. C. Richards, *Principles of Powder Mechanics* (Pergamon Press, Oxford, 1970).
[2] H. M. Jaeger, S. R. Nagel, and R. P. Behringer, Rev. Mod. Phys. **68**, 1259 (1996).
[3] J. Duran, *Sands, Powders, and Grains: An Introduction to the Physics of Granular Materials* (Springer, New York, 2000).
[4] J. S. Uehara, M. A. Ambroso, R. P. Ojha, and D. J. Durian, Phys. Rev. Lett. **90**, 194301 (2003); **91**, 149902(E) (2003).
[5] K. A. Newhall and D. J. Durian, Phys. Rev. E **68**, 060301R (2003).
[6] R. W. Nelson, Phys. Today **56**, 32 (2003).
[7] S. Thoroddsen and A. Shen, Phys. Fluids **13**, 4 (2001).
[8] D. Lohse, R. Bergmann, R. Mikkelsen, C. Zeilstra, D. van der Meer, M. Versluis, K. van der Weele, M. van der Hoef, and H. Kuipers, Phys. Rev. Lett. **93**, 198003 (2004).
[9] *Impact and Explosion Cratering*, edited by D. J. Roddy, R. O. Pepin, and R. B. Merril (Pergamon Press, New York, 1978).
[10] H. J. Melosh, *Impact Cratering: A Geologic Process* (Oxford University Press, New York, 1989).
[11] K. Holsapple, Annu. Rev. Earth Planet Sci. **21**, 333 (1993).
[12] J. Amato and R. Williams, Am. J. Phys. **66**, 141 (1998).
[13] Y. Grasselli and H. Herrmann, Granular Matter **3**, 201 (2001).
[14] A. M. Walsh, K. E. Holloway, P. Habdas, and J. R. de Bruyn, Phys. Rev. Lett. **91**, 104301 (2003).
[15] X.-J. Zheng, Z.-T. Wang, and Z.-G. Qiu, Eur. Phys. J. E **13**, 321 (2004).
[16] D. Gidaspow, *Multiphase Flow and Fluidization: Continuum and Kinetic Theory Descriptions* (Academic Press, Boston, 1994).
[17] M. P. Ciamarra, A. H. Lara, A. T. Lee, D. I. Goldman, I. Vishik, and H. L. Swinney, Phys. Rev. Lett. **92**, 194301 (2004).
[18] J. R. de Bruyn and A. M. Walsh, Can. J. Phys. **82**, 439 (2004).
[19] D. Lohse, R. Rauhe, R. Bergmann, and D. van der Meer, Nature (London) **432**, 689 (2004).
[20] R. P. Ojha, N. Menon, and D. J. Durian, Phys. Rev. E **62**, 4442 (2000).
[21] I. Albert, J. G. Sample, A. J. Morss, S. Rajagopalan, A. L. Barabasi, and P. Schiffer, Phys. Rev. E **64**, 061303 (2001), and references therein.
[22] M. B. Stone, D. P. Bernstein, R. Barry, M. D. Pelc, Y. K. Tsui, and P. Schiffer, Nature (London) **427**, 503 (2004).